Measurement of Interfacial Area per Volume for Drainage and Imbibition

Daiquan Chen[1]*, Laura J. Pyrak-Nolte[1, 2] , Jessica Griffin [2], and Nicholas J. Giordano [2]
[1]*Department of Earth and Atmospheric Sciences*
[2]*Department of Physics*
Purdue University, West Lafayette, Indiana USA

**Currently at Petroleum Abstracts, The University of Tulsa, Tulsa, OK USA*

Abstract: We investigate experimentally the functional relationship among capillary pressure, P_c, wetting phase saturation, S_w, and interfacial area per volume between the wetting and non-wetting phases, a_{wn}, for drainage and imbibition processes in micro-models of two-dimensional pore structures. Within the experimental and analysis error (around 10%-15%), the resulting P_c-S_w-a_{wn} surfaces were the same. This suggests that data obtained from either the drainage process or the imbibition process are sufficient to generate the complete functional relationship among P_c-S_w-a_{wn}, and that the observed hysteresis in P_c-S_w-a_{wn}, can be modeled by including interfacial area as an additional state variable

Introduction

The study of the flow of multiple fluid phases in a porous medium has application in many disciplines such as oil, gas, and water recovery, ground water protection as well as micro-fluidic biosensor chips. For some of these applications, measurements of hydraulic parameters on the laboratory scale (pore- to core-scale) are often made to predict multiphase fluid movement on larger scales. This raises the question of how pore-scale information can be up-scaled to macro-scale measurements. Several investigators (Gvirtzman & Roberts, 1991; Hassanizadeh & Gray, 1990; Bradford & Leij, 1997; Deinert et al., 2005) have recognized that an accurate description of multiphase flow in a porous medium must account for the thermodynamics and the geometry of the interfaces between the fluids (and between the fluids and the solid phase). The theoretical motivation for including interfacial area per volume in the capillary pressure - saturation relationship is based on the way capillary pressures are defined on the pore scale and how they relate to the macro-scale measurements of capillary pressures and saturations. On the pore scale, the capillary pressure between a wetting phase, *w*, fluid and a non-wetting, *n*, phase fluid is given by

$$P_c = \gamma^{wn}\left(\frac{1}{R_1}+\frac{1}{R_2}\right) = \gamma^{wn} J \qquad (1)$$

where γ^{wn} is the interfacial tension between the wetting and non-wetting phase and J is the mean curvature of the interfaces based on the principal radii of curvature of the surface, R_1 and R_2. This relation shows how P_c depends on the geometry of the interfaces. Capillary pressure at equilibrium P_{ceq} can also be defined as a balance of forces between the fluids on either side of the interfaces and is defined as

$$P_{ceq} = P_n - P_w \qquad (2)$$

The equation for P_{ceq} is generally assumed to be applicable on the macro-scale (core or field scale) as long as P_{ceq} is taken to be a function of the wetting phase saturation, S_w. However, it has been shown by numerous experimental investigations that P_{ceq} has a hysteretic relationship with saturation, i.e. the capillary pressure - saturation relationship depends on the drainage and imbibition history of the system and is not a single valued function (Morrow, 1965; Topp, 1969; Colonna et al., 1972; Collins, 1974; Lenhard, 1992). Hence, capillary pressure cannot be determined simply from saturation or vice versa.

Hassanizadeh and Gray (1990 & 1993) proposed that the capillary pressure - saturation relationship is a two-dimensional projection of a more extensive functional dependence, i.e., a third variable is needed to explicitly define the state of the system. They propose that the third variable is interfacial area per volume (IAV). For any porous system with wetting and non-wetting phases, three interfacial areas can be defined: between the two fluid phases and between each fluid phase and the solid. The IAV that is important to the capillary pressure – saturation relationship is the IAV between the wetting phase and the non-wetting phase which we denote as a_{wn}. a_{wn} is a parameter that depends on the distribution of the fluid phases within the system.

Reeves et al. (1996) used a numerical model to study the role of a_{wn} in multiphase flow using a pore-scale network model to simulate both drainage and imbibition processes. Their model found a difference between the P_c-S_w-a_{wn} surfaces for these two processes. For example, the maximum value of a_{wn} during drainage occurs at a wetting phase saturation just below 50%. For imbibition, a_{wn} reaches a the maximum value at a significantly lower wetting phase saturation of around 37%.

Held and Celia (2001) also investigated, numerically, the functional relationship among capillary pressure, saturation and interfacial area using a pore-scale network model. They used the same drainage mechanism as Reeves et al.(1996), but employed a different imbibition mechanism. They considered the effects of snap-off of non-wetting phase and local fluid configurations during imbibition. To compare surfaces from drainage and imbibition, Held & Celia (2001) used normalized moments of residuals, with the normalization performed with respect to the area of the main hysteresis loop in the pressure-saturation plane. They observed that the P_c-S_w-a_{wn} surfaces generated for drainage scanning and imbibition scanning lie on the same surface to within 1.5% when the optimized snap-off and local configuration parameters are selected to minimize the hysteresis.

Cheng (2002) and Cheng et al. (2004) made measurements of a_{wn}, P_c and S_w on two-dimensional micro-models to determine if a_{wn} does indeed lift the ambiguity in the capillary pressure – saturation relationship. They found that although each 2D projection of the surface was hysteretic, the complete three-dimensional surface is invertible for their dataset. They observed that when multiple data fall within small regions of the P_c-S_w plane, they had similar a_{wn} values within the experimental error. However, their measurements were made only for imbibition scanning. If the surface is truly unique, then both imbibition and drainage scanning curves should lie on the same surface. In this technical note, we present the results of an experimental investigation of two-dimensional micro-models to determine if the capillary pressure – saturation - IAV surface acquired through drainage and imbibition scanning do indeed lie on the same surface.

Micro-Model Sample Fabrication and Experimental Set-up

Transparent micro-fluidic cells, referred to as micro-models, were used to investigate the relationship among capillary pressure, saturation and interfacial area per volume for imbibition and drainage processes. The micro-models were fabricated using the optical lithography methods described in Cheng (2002) and Cheng et al (2004). In this approach, a base slide is spin-coated with a UV sensitive polymer (Shipley 1827 photoresist) to an approximate thickness of either 1 micron or 2 microns. Photolithography is used to create the inlet and outlet regions of the sample as well as the two-dimensional porous structure. The micro-model is sealed by bonding a glass cover slide that was spin-coated with a very thin layer (approximately 0.2 micron) of Shipley 1805 photoresist. Three micro-models were constructed for this study and the porosity of each sample is given in Table 1. Figures 1a, 1b and 1c are the images of the samples saturated with nitrogen. The porous structures are 600 microns on a side and their depths are given in Table 1.

A fluid displacement system was used to introduce two fluid phases into the micro-models. The system simultaneously measures the pressure and images the fluid distribution within the porous structure. The system contains (1) a Qimaging Retica EX CCD camera to take digital images through an Olympus microscope with a 16x objective and (2) an Omega PX5500C1-050GV pressure transducer to measure the nitrogen

pressure at the sample inlet. The outlet was exposed to atmospheric pressure.

To perform a measurement on a micro-model, the micro-model is initially saturated with a wetting fluid, decane, which is inserted through the outlet region with a syringe. For the drainage process, nitrogen (non-wetting phase) is invaded into the micro-model by increasing the nitrogen pressure on the inlet side. Conversely, for the imbibition process, the nitrogen pressure on the inlet side of the sample is decreased. Scanning imbibition curves are generated by stopping at a point on the main drainage loop and then incrementally decreasing the pressure of the non-wetting phase, always returning to the lowest pressure used. The drainage scanning curves are generated by stopping at a point on the main imbibition loop and then incrementally increasing the pressure of the non-wetting phase, always returning to the highest pressure possible without causing breakthrough. After each pressure increment, the system is allowed to equilibrate, typically taking 5 minutes, and the saturation and distribution of each phase are digitally imaged while the inlet pressure is recorded. The maximum pressure is controlled to be very close to (but less than) the breakthrough pressure so the non-wetting phase never flows through the micro-model but fills the pore space as much as possible. All measurements are conducted at room temperature (temperature stability better than 0.5 degree Celsius during a measurement), with the apparatus located within a clean bench environment. For the imbibition process, the pressure is incrementally decreased to allow the nitrogen to drain from the sample. Again, the system is allowed to equilibrate prior to recording the data. Table 1 also lists the number of images taken for imbibition and drainage measurements for each sample. An archive of the images used in this study have been placed on a website for downloading (see reference Pyrak-Nolte, 2007).

Data Analysis

The digital images of the fluid distributions in the micro-models are analyzed with custom IDL programs to determine saturation and interfacial area per volume at each pressure. From the images, interfacial length is measured instead of interfacial area because the images are two-dimensional. We use the interfacial length between the wetting and non-wetting phase as an approximation for a_{wn}. Though the length of the hidden curvature should be constant factor (because the depth of the pore structure is constant), a_{wn} does not include the length of the hidden curvature because it could not be directly measured from the images. The resolution of an image is 0.6 micron per pixel edge length. In the analysis, each phase (wetting, non-wetting and solid phases) is identified. After all three phases in an image are detected, the saturation of any one phase can be calculated by counting the pixels for a given fluid phase and dividing by the pore space area. A Sobel edge detector is used to identify interfaces between the phases. The edge length between the wetting and non-wetting phases, L_{wn}, is calculated based on the edge lengths of wetting, w, non-wetting, n, and solid, s, phases by using equation:

$$L_{wn} = (L_w + L_n - L_s)/2 \qquad (3)$$

The interfacial area per volume is found by dividing L_{wn} by the total area of the micro-model (600 microns by 600 microns) giving units of inverse length. Chen (2006) considered the error in L_{wn} resulting from our image analysis technique from two test cases: (1) different squares with known areas and perimeters; and (2) different circles with known areas and circumferences. For squares, the relative error between the estimated and the known areas of squares is small, i.e., very close to zero. For circles, the error is around 5 % when the radius of the circle is less than 13 pixels. When the radius of the circle is greater than 13 pixels, the error is almost zero.

The error in calculating interfacial area per volume based on equation (3) was determined based on the two test cases. The relative error between the estimated and the known perimeter of the squares is the largest (-30% to -10%) when the edge length is less than 4 pixels but decreases quickly (~ 5% at 6 pixels) as the perimeter increases. The relative error between the estimated and the known circumferences of circles is large (-20%) when the radius of the circle is less than 4 pixels but decreases quickly to 10% as the radius increases. The error in the circumference is large at small radii because the smoothness of the circumference of the circle is reduced (or

pixilated) when composed of few pixels (i.e., squares)

These two test cases point out that the error in saturation and IAV from the analysis depends not only on the resolution but also on the curvature of the border of a phase. When high-resolution images are used, the error in saturation is small, less than 1 per cent. But in the worst case, the maximum error of IAV may be as high as 10% and tends to be underestimated. Other methods exist for determining interfacial areas (e.g. Dalla et al., Mclure et al, 2006; Prodanovic et al., 2006) that might reduce the error but at this time we chose the simplest analysis method.

The relations for the edge length calculations were also applied to several numerical test cases. When the edge was a straight line, the result was the same as the real length. For curve-linear features, at most a 10% loss in edge length was calculated. In the test cases, the estimation of the saturation of each phase was very accurate. Even in the worst case, the loss in saturation was less than 1%.

We use a ratio approach to compare the P_c-S_w-a_{wn} surfaces for drainage and imbibition to the measured data points. For each process (imbibition and drainage) a surface is fitted to P_c, S_w, and a_{wn} data where the subscript *wn* stands for the interface between the wetting and non-wetting phases. The surfaces are fitted using two procedures in IDL: (1) TRIANGULATE and (2) TRIGRID. The measured values of P_c and S_w do not fall on a regular grid. The TRIANGULATE procedure uses a Delaunay triangulation of a planar set of points to create a regular grid from irregularly gridded data points (in this case P_c and S_w) . The output from TRIANAGULATE is used in the TRIGRID procedure along with the data for P_c, S_w, and a_{wn}. The TRIGRID procedures returns a regular grid of interpolated Z values (in this case a_{wn}). For this study, the linear interpolation option of the TRIGRID procedure was selected and no extrapolation outside of the triangulation was used. The following options were selected when using the TRIGRID function: (a) GS which sets the spacing between grid points (Table 2); (b) LIMITS which specifies the data range to be gridded (Table 2); (c) NX & NY which specifies the output grid size in the x and y direction; and (d) XGRID and YGRID were set to named variables that contained the x and y values of the output grid. The limits for the capillary pressure and saturation were chosen to be slightly larger than the minimum and maximum values of the data for each sample and differed among samples. However, the same limits were used for both imbibition and drainage surfaces for a given sample. The spacing between grid points, GS, was chosen based on the limits, NX and NY. The values of NX and NY were set to a value of 55 for all samples and for both drainage and imbibition.

To determine whether data acquired through imbibition scanning and drainage scanning lie on the same surface, the following ratio was calculated

$$R = \frac{a_{data}(s,p)}{a_{int}(s,p)} \qquad (4)$$

where a_{data} is the measured interfacial area per volume between the wetting and non-wetting phases from the micro-model data, and a_{int} is the interfacial area per volume between the wetting and nonwetting phases from the interpolated surfaces. Equation (4) is applied to the measured values of P_c-S_w-a_{wn} and the interpolated surfaces generated from the data from samples S1dc, S3jg and S6dc. The ratio was used to determine the quality of the fit of the interpolated surface to the data for each process (Table 3), as well as to determine how well the imbibition data lie on the interpolated drainage surface (and conversely how well the drainage data lie on the interpolated imbibition surface).

Results and Discussion

Figures 2a, 2b and 2c show the imbibition and drainage scanning curves of samples S1dc, S6dc and S3jg, respectively, in the saturation-pressure plane. In Figure 3, the color of the symbols represents the value of a_{wn} that was determined from the images. The scanning curves for these three samples are substantially different because of the different porosities (Table 1) and other differences in pore structure. Note that there are some regions of the pore structure that are not accessed by the non-wetting phase during either the drainage or imbibition processes, i.e. the gaps in the scanning curves. The maximum a_{wn} is approximately 6040/m, 4310/m and 2180/m for samples S1dc, S3jg, and S6dc, respectively. Several other studies have investigated a_{wn} as a

function of saturation and pressure using a variety of techniques (Kim et al.; 1997; Saripalli et al., 1997; Costanza-Robinson & Brusseau, 2002; Culligan et al. 2004 & 2006; Chen & Kibbey, 2006). Saripalli et al. (1997) determined a value of a_{wn} = 13000/m for a air-water phases in a sand for a water saturation of 35%. On the other hand, Culligan et al. (2004; 2006) determined a maximum value of a_{wn} of 250/m for oil-water interface and 390/m for air-water interface in a glass bead pack. The maximum a_{wn}, for samples S1dc, S3jg and S6dc, occurs during imbibition at low wetting phase saturations and somewhat low capillary pressures (Figure 2). The maximum value of a_{wn} is observed to increase with increasing porosity. The magnitude of a_{wn} for the micro-model differs from those mentioned above for several reasons, namely, the porosity of the sample (Table 1), not accounting for the hidden curvature and some techniques include a_{wn} associated with films (e.g., Chen and Kibbey, 2006) which we do not.

Figures 3a, 3b and 3c contain graphs of R (from equation 4) as a function a_{wn} two cases: (1) $R_{imb} = a_{data,imb}/a_{int,dra}$ as a function of $a_{wn} = a_{data,imb}$ and (2) $R_{dra} = a_{data,dra}/a_{int,imb}$ as a function of a $a_{wn} = a_{data,dra}$. For both cases, a_{wn} is the interfacial area between the wetting and non-wetting phases and does not include regions associated with films. With this method, experimentally measured data points are compared to the value of a_{wn} from the interpolated surface with same value of P_c and S_w. to within 0.2% and 0.5%, respectively. The values of P_c and S_w from the data cannot be exactly matched to the interpolated surface value because the interpolated surfaces are regularly gridded. If R = 1, then the data and value from the interpolated surface are the same.

Figures 3a, 3b and 3c also contain the histogram of R (on the right vertical axis and top horizontal axis). The mean and standard deviation of the histogram are given in Table 3 for all samples. Also given in Table 3 is the average R values and standard deviation in R values for each data set compared to its own interpolated surface as measure of the quality of fit. By comparing the mean and standard deviation of the R values for imbibition and drainage data compared to the opposite surface (e.g., imbibition data compared to interpolated drainage surface), it is observed that the data do indeed lie on the interpolated surface to within the experimental/analysis error. The standard deviations in R_{imb} (column 3 in Table 3) and R_{dra} (column 4 in Table 3) are similar to those for imbibition data compared to the interpolated imbibition surfaces (column 1 in Table 3) and for drainage data compared to the interpolated drainage surfaces (column 2 in Table 3).

From Figure 2a and Table 3, the imbibition and drainage surfaces are the same to within $\pm$10% for sample S1dc. The histograms for samples S3jg and S6dc (Figures 2b & 2c) exhibit a broader distribution of R values. The standard deviations (Table 3) for S3jg and S6dc between the imbibition and drainage behavior range from $\pm$10% to $\pm$15%. From the graphs of R as a function a_{wn} in Figure 3, the largest deviations from the surfaces occur at low values of a_{wn} which occur mainly at wetting phase saturations greater than 0.9. When nitrogen is first entering the micro-model, i.e. for wetting phase saturations between 0.9 and 1.0, a competition between flow paths leads to an instability causing the fluid distribution for these saturations to vary on each drainage cycle.

Conclusion

The experimentally determined P_c-S_w- a_{wn} surfaces show that each micro model has its own unique surface. The quality of fit for the surface through the data points is on the same order of magnitude as that from the comparison of the imbibition data to the interpolated drainage surface and also for the comparison of the drainage data to the interpolated imbibition surface. For each sample, within the experimental error, the difference between the drainage and the imbibition processes is small for the specific wetting and non-wetting phases used in these micro-model experiments

Earlier, Cheng et al. (2004) stated that the P_c-S_w- a_{wn} surfaces were unique to within 5%. Their value was not based on comparing imbibition and drainage surfaces but was arrived at from an analysis of a single surface. In this current study, the differences between imbibition and drainage surfaces is around 10%-15% but still within the experimental error (from image analysis, surface fitting, etc.), and suggests that the P_c-S_w- a_{wn} surface may indeed be unique. This suggests that data from either drainage scans or imbibition scans

may be sufficient to determine the functional relationship among P_c-S_w- a_{wn} for a porous medium.

These results also suggest that the observed hysteresis in P_c-S_w- a_{wn} can be modeled by including interfacial area as an additional state variable. Recently, Chen & Kibbey (2006) stated that P_c-S_w- a_{wn} is not unique based on data from a surface active tracer technique applied to two fluid phases in a fine sand. However, in their analysis they included interfacial area from films which are not included in our calculation of a_{wn}. We do not include the contribution to a^{wn} from films because as discussed in Cheng et al. (2004), including disjoining-pressure-dominated interfaces (such as those interfaces between a bulk fluid and a fluid film) leads to a linear dependence between S_w- a_{wn} and a_{wn} does not provide any additional information. However, Cheng et al. (2004) showed that it is only the capillary-dominated interfaces (interface between bulk fluids) that lifts the ambiguity in the P_c-S_w hysteresis. Thus the uniqueness of the P_c-S_w- a_{wn} relationship cannot be determined from techniques that cannot distinguish between capillary-dominated interfaces and disjoining-pressure-dominated interfaces.

Finally, future work research must repeat these experiments on three-dimensional porous systems to verify that the observed behavior we have found for these low dimensional systems can be applied to three-dimensional systems.

Acknowledgments: The authors wish to acknowledge useful discussions with David D. Nolte. This material is based upon work supported by the National Science Foundation under Grant No. 0509759.

References

Bradford, S.A., and F. J. Leij, 1997, Estimating interfacial areas for multi-fluid soil systems, *Journal of Contaminant Hydrology*, *27*, 83-105

Chen, D., 2006, Experimental investigation of interfacial geometry associated with multiphase flow within a porous medium, Ph.D. Thesis, Department of Earth and Atmospheric Sciences, Purdue University, West Lafayette, Indiana.

Chen, L. and T. C. G. Kibbey, 2006, Measurement of Air-Water Interfacial Area for Multiple Hysteretic Drainage Curves in an Unsaturated Fine Sand, Langmuir 2006, 22, 6874-6880

Cheng, J., 2002, Fluid flow in ultra-small structures, Ph.D. Thesis, Department of Physics, Purdue University, West Lafayette, Indiana.

Cheng J.&-T., L. J. Pyrak-Nolte, D. D. Nolte, N. J. Giordano, 2004, Linking pressure and saturation through interfacial areas in porous media, *Geophys. Res. Let.*, *31*, L08502, doi:10.1029/2003GL019282.

Colonna, J., Brissaud, F. and Millet, J.L., 1972. Evolution of capillary and relative permeability hysteresis. Soc. Pet. Eng. J., 12: 28-38.

Costanza-Robinson, M.S., and M. L. Brusseau, 2002, Air-water interfacial areas in unsaturated soils: Evaluation of interfacial domains. Water Resources Research, 2002. **38**(10): p. 1195 doi: 10.1029/2001WR000738.

Culligan, K.A., D. Wildenschild, B.S.B. Christensen, W.G. Gray, and M.L. Rivers, 2005. Pore-scale Characteristics of Multiphase Flow in Porous Media: A Synchrotron-based CMT Comparison of Air-Water and Oil-Water Experiments. Advances in Water Resources. 29(2), 227-238.

Culligan, K.A., D. Wildenschild, B.S.B. Christensen, W.G. Gray, A.F.B. Tompson, 2004. Interfacial Area Measurements for Unsaturated Flow Through a Porous Medium. Water Resources Research. 40(12), Art. No. W12413, Dec 22.

E. Dalla, M. Hilpert , and C. T. Miller, 2002, Computation of the interfacial area for two-fluid porous medium systems, Journal of Contaminant Hydrology 56, 25– 48

Deinert, M. R., Parlange, J.-Y., and K. B. Kady, 2005, Simplified thermodynamic model for equilibrium capillary pressure in a fractal porous medium, *Physical Review E, 72*, 041203.

Gvirtzman H., and P.V. Roberts, 1991, Pore scale spatial analysis of two immiscible fluids in porous media, *Water Resources Research*, *27(6)*, 1165-1176.

Hassanizadeh, S.M. and W.G. Gray, 1990, Mechanics and thermodynamics of multiphase flow in porous-media including interphase

boundaries. *Advances in Water Resources*, *13(4)*, 169-186.

Held, R. J. and Celia, M. A., 2001, Modeling support of functional relationships between capillary pressure, saturation, interfacial area and common lines, *Advances in Water Resources*, *24*, 325-343.

Kim, H., Rao, P.S.C., and M. D. Annable, 1997, Determination of effective air-water interfacial area in partially saturated porous media using surfactant adsorption, *Water Resource,* 33(12), 2705–2711.

Lenhard, R. J., 1992, Measurement and modeling of three-phase saturation-pressure hysteresis *Journal of Contaminant Hydrology,* 9, 243-269

McClure J.E., Adalsteinsson, D., Pan C, Gray, W.G. and C.T. Miller, 2007, Approximation of interfacial properties in multiphase porous medium systems, Advances in Water Resources 30, 354–365

Morrow, N.R., 1965. Capillary equilibrium in porous materials. Soc. Pet. Eng. J., 5: 15-24.

Prodanovic, M., W.B. Lindquist , and R.S. Seright, 2006, Porous structure and fluid partitioning in polyethylene cores from 3D X-ray microtomographic imaging, Journal of Colloid and Interface Science 298, 282–297

Pyrak-Nolte, L. J., 2007, URL of website with original data: http://www.physics.purdue.edu/rockphys/DataImages/

Reeves, P. C. and Celia, M. A., 1996, A functional relationship between capillary pressure, saturation, and interfacial area as revealed by a pore-scale network model, *Water Resources Research*, *32*(8), 2345-2358.

Saripalli, K.P., Kim, H., Rao, P.S.C., Annable, M.D., 1997, Measurement of specific fluid-fluid interfacial areas of immiscible fluids in porous media. Environmental Science and Technology, **31**(3), 932-926

Topp, G.C., 1969. Soil-water hysteresis measured in a sandy loam and compared with the hysteretic domain model. Soil Sci. Soc. Am. Proc., 33: 645-651.

Table 1. The parameters of the samples used to compare imbibition and drainage measurements

Sample ID	Porosity	Channel Depth (microns)	Number of images for imbibition	Number of images for drainage
S1dc	0.703	1	205	206
S3jg	0.514	2	1220	498
S6dc	0.556	1	187	191

Table 2. The parameters used in the TRIGRID function for interpolating the P_c, S_w and a_{wn} surfaces for drainage and imbibition. Min and max refer to the minimum and maximum values of the parameter.

Sample ID	LIMITS Capillary Pressure [min, max] (kPa)	LIMITS Wetting Phase Saturation [min, max]	GS: Spacing between Saturation Grid Points	GS: Spacing between Capillary Pressure Grid Points (kPa)
S1dc	50.0, 56.0	0.45, 1.0	0.01	0.1
S3jg	28.0, 34.0	0.76, 1.0	0.00436	0.1
S6dc	48.0, 57.0	0.74, 1.0	0.0047	0.1

Table 3. Averages and Standard Deviations (in parentheses) of R (equation 4) for comparison of data to interpolated surfaces using linear interpolation.

Sample	$a_{data,imb}/a_{int,imb}$	$a_{data,dra}/a_{int,dra}$	$R_{imb} = a_{data,imb}/a_{int,dra}$	$R_{dra} = a_{data,dra}/a_{int,imb}$
S1dc	0.99 (0.05)	0.99 (0.04)	0.96 (0.08)	1.03 (0.07)
S3jg	0.98 (0.14)	0.97 (0.08)	1.01 (0.15)	0.94 (0.10)
S6dc	0.96 (0.09)	1.01 (0.07)	0.98 (0.12)	1.10 (0.16)

(a) S1dc

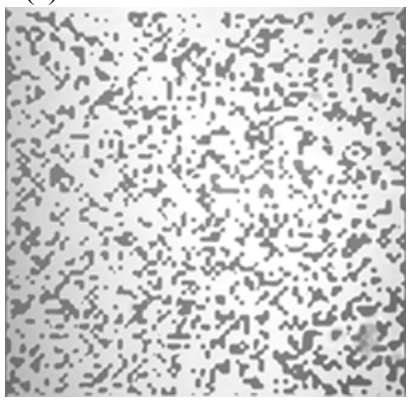

(b) S3jg

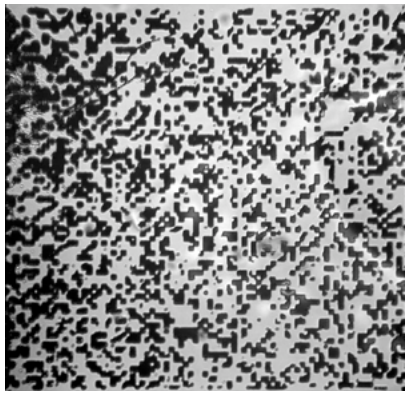

(c) S6dc

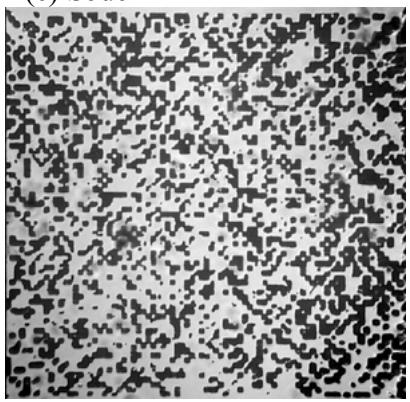

Figure 1. Digital images of micro-model samples (a) S1dc, (c) S3jg and (c) S6dc. In the digital images, white regions represent the pore space and black regions represent grains.

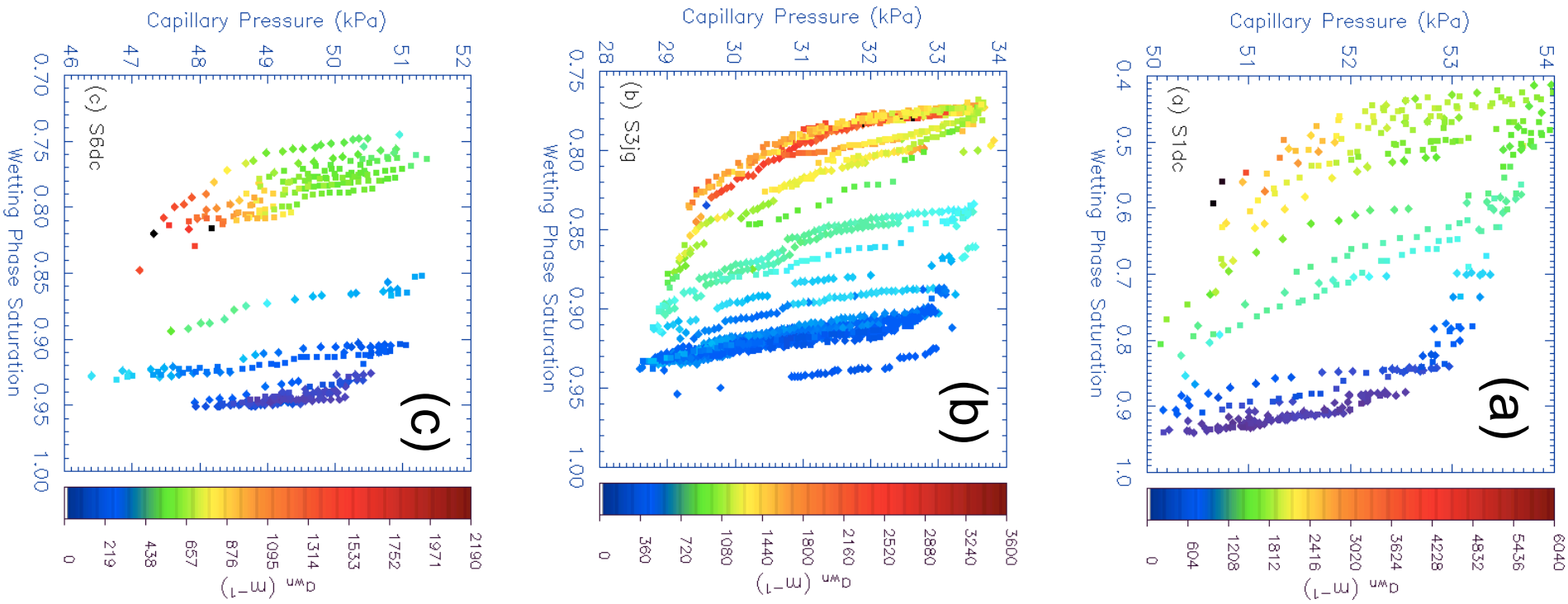

Figure 2. Capillary pressure - saturation relationship for imbibition (filled squares) and drainage (filled diamonds) for samples (a) S1dc, (b) S3jg, and (c) S6dc. The color scale represents the value of a_{wn} (in units of 1/m) for each point.

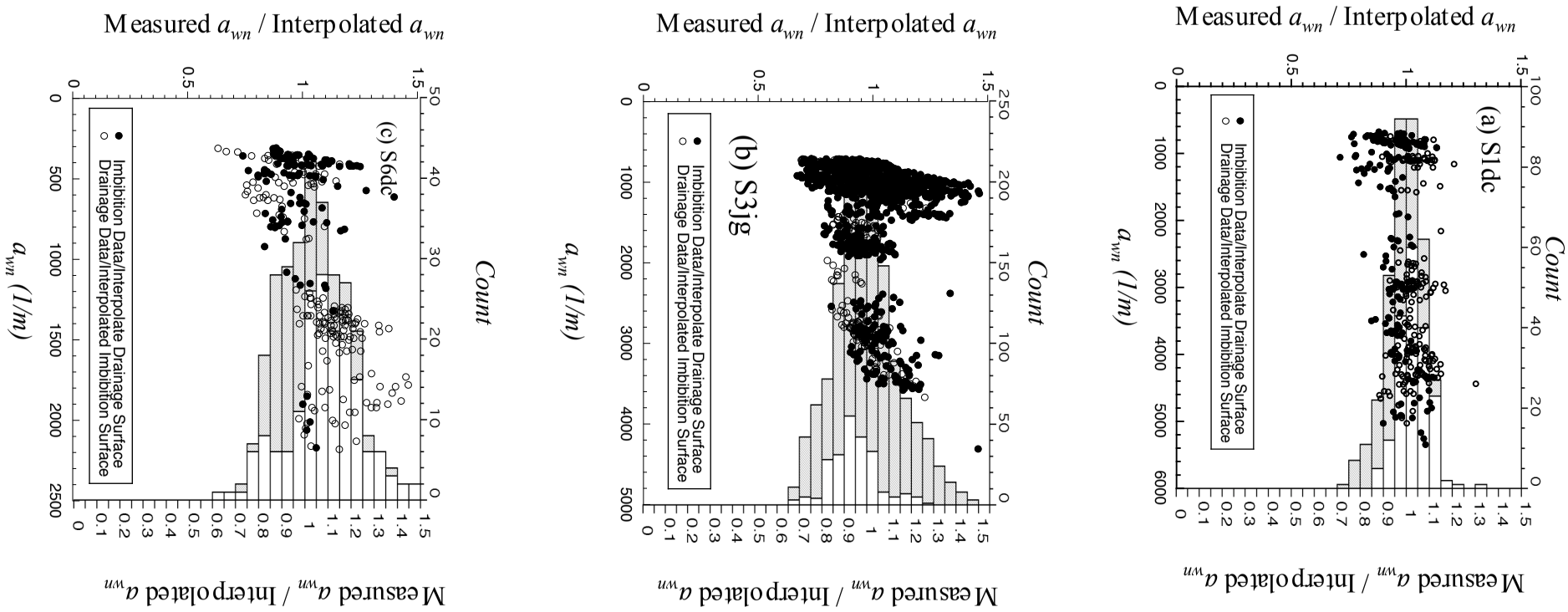

Figure 3. The ratio (equation 4) of measured a_{wn} to the a_{wn} from the interpolated surfaces as a function of a_{wn} for samples (a) S1dc, (b) S3jg and (c) S6dc is shown on the right vertical axis (Measured a_{wn}/Interpolated a_{wn}) and the lower horizontal axis (a_{wn}). The histogram of the ratio is shown using the right vertical axis (Measured a_{wn}/Interpolated a_{wn}) and the top horizontal axis (count). In the histogram, the gray shaded bars represent the R values for imbibition data compared to the interpolated drainage surface, and the white bars represent the R values for the drainage data compared to the interpolated imbibition surface.